Scanning Electrochemical Microscopy. 59. Effect of Defects and Structure on Electron Transfer through Self-Assembled Monolayers

Abolfazl Kiani,[†,‡] Mario A. Alpuche-Aviles,[†] Paul K. Eggers,[§] Michael Jones,[§] J. Justin Gooding,[§] Michael N. Paddon-Row,[§] and Allen J. Bard*[,†]

Center for Electrochemistry, Chemistry and Biochemistry Department, The University of Texas at Austin, Austin, Texas 78712, and School of Chemistry, University of New South Wales, Sydney, New South Wales 2052, Australia

Received September 10, 2007. In Final Form: November 26, 2007

Electron transfer (ET) rate kinetics through *n*-alkanethiol self-assembled monolayers (SAMs) of alkanethiols of different chain lengths [$Me(CH_2)_nSH$; $n = 8, 10, 11, 15$] on Au and Hg surfaces and ferrocene (Fc)-terminated SAMs (poly-norbornylogous and $HS(CH_2)_{12}CONHCH_2Fc$) on Au were studied using cyclic voltammetry and scanning electrochemical microscopy (SECM). The SECM results allow determination of the ET kinetics of solution-phase $Ru(NH_3)_6^{3+/2+}$ through the alkanethiol SAMs on Au and Hg. A model using the potential dependence of the measured rate constants is proposed to compensate for the pinhole contribution. Extrapolated values of k^o_{ML} for $Ru(NH_3)_6^{3+/2+}$ using the model follow the expected exponential decay (β is 0.9) for different chain lengths. For a Fc-terminated poly-norbornyl SAM, the standard rate constant of direct tunneling (k^o is 189 ± 31 s^{-1}) is in the same order as the k^o value of $HS(CH_2)_{12}CONHCH_2Fc$. In blocking and Fc SAMs, the rates of ET are demonstrated to follow Butler−Volmer kinetics with transfer coefficients α of 0.5. Lower values of α are treated as a result of the pinhole contribution. The normalized rates of ET are 3 orders of magnitude higher for Fc-terminated than for blocking monolayers. Scanning electron microscopy imaging of Pd nanoparticles electrochemically deposited in pinholes of blocking SAMs was used to confirm the presence of pinholes.

Introduction

Long-range electron transfer (ET) has been widely studied in chemical and biological systems. The effect of the linking group (or bridge) that separates the electron acceptor and donor sites on ET is of fundamental interest in chemistry, as ET rates appear to be a function of the structure and composition of the bridge. This topic is also of interest for potential applications, for example, in surface passivation and molecular electronics. Numerous electrochemical experiments have been carried out to study the effects of bridge composition on ET through self-assembled monolayers (SAMs) of alkanethiols, which spontaneously form highly ordered monolayers on Au and Hg surfaces.[1,2] SAMs allow a high degree of distance control, which can be varied with a resolution of about one bond length (~1.5 Å per CH_2 group).[3] The chemical composition of the bridge can also be varied to determine the ET dependence on structure. Investigations of monolayers (e.g., of alkanethiols) have been described in a number of papers and reviews,[1,2] and ET through these SAMs has been measured by chronoamperometry (CA),[4,5] cyclic voltammetry (CV),[6−9] impedance spectroscopy,[10,11] potentiometry,[12] and scanning electrochemical microscopy (SECM).[13,14]

In one approach to ET measurements of solution species with SAMs, the molecules self-assembled on the surface of a metal (e.g., Au or Hg) via a thiol group, with the terminal end of the molecule being a group that is not electrochemically active (e.g., a methyl or carboxyl group). The rate of ET to a redox mediator in solution (e.g., $Ru(NH_3)_6^{3+}$ or $Fe(CN)_6^{4-}$) through the blocking SAM was then measured. The rate constants at given potentials (k_{ML}) were used to determine the standard rate constant (k^o_{ML}), at E^o for the redox mediator, and the transfer coefficient, α, for different SAM thicknesses and structures. In such studies, deviations of the potential dependence of k_{ML} (represented by α) from the expected value of ~0.5 have often been observed, and attempts have been made to explain this deviation theoretically.[6,7] However, an important uncertainty in such studies is the need to assume defect- or pinhole-free SAMs since ET occurring at such sites will provide a parallel path that is faster than that through the monolayer itself. As discussed next, pinholes can contribute to the electrochemical measurement and result in inaccurate kinetic data.

The effect of defects and pinholes has been treated as an ultramicroelectrode (UME) array.[15] Reports in the literature describe methods for detecting pinholes on SAMs either by

* Corresponding author. E-mail: ajbard@mail.utexas.edu.
† The University of Texas at Austin.
‡ Current Address: Department of Chemistry, Faculty of Science, University of Isfahan, Isfahan, Iran.
§ University of New South Wales.

(1) Finklea, H. O. Electrochemistry of organized monolayers of thiols and related molecules on electrodes. In *Electroanalytical Chemistry*; Bard, A. J., Rubinstein, I., Eds.; Marcel Dekker: New York, 1996; Vol. 19, pp 109−335.
(2) For reviews see: (a) Ulman, A. *Chem. Rev.* **1996**, *96*, 1533−1554. (b) Love, J. C.; Estroff, L. A.; Kriebel, J. K.; Nuzzo, R. G.; Whitesides, G. M. *Chem. Rev.* **2005**, *105*, 1103−1169.
(3) Porter, M. D.; Bright, T. B.; Allara, D. L.; Chidsey, C. E. D. *J. Am. Chem. Soc.* **1987**, *109*, 3559−3568.
(4) Chidsey, C. E. D. *Science (Washington, DC, U.S.)* **1991**, *251*, 919−922.
(5) Smalley, J. F.; Finklea, H. O.; Chidsey, C. E. D.; Linford, M. R.; Creager, S. E.; Ferraris, J. P.; Chalfant, K.; Zawodzinsk, T.; Feldberg, S. W.; Newton, M. D. *J. Am. Chem. Soc.* **2003**, *125*, 2004−2013.
(6) Miller, C.; Cuendet, P.; Grätzel, M. *J. Phys. Chem.* **1991**, *95*, 877−886.
(7) Miller, C.; Grätzel, M. *J. Phys. Chem.* **1991**, *95*, 5225−5233.
(8) Demoz, A.; Harrision, D. J. *Langmuir* **1993**, *9*, 1046−1050.
(9) Tender, L.; Carter, M. T.; Murray, R. W. *Anal. Chem.* **1994**, *66*, 3173−3181.
(10) Lesia, V.; Protsailo, W.; Fawcett, R. *Electrochim. Acta* **2000**, *45*, 3497−3505.
(11) Cohen-Atiya, M.; Nelson, A.; Mandler, D. *J. Electroanal. Chem.* **2006**, *593*, 227−240.
(12) Cohen-Atiya, M.; Mandler, D. *Phys. Chem. Chem. Phys.* **2006**, *8*, 4405−4409.
(13) Forouzan, F.; Bard, A. J.; Mirkin, M. V. *Isr. J. Chem.* **1997**, *37*, 155−163.
(14) Liu, B.; Bard, A. J.; Mirkin, M. V.; Creager, S. E. *J. Am. Chem. Soc.* **2004**, *126*, 1485−1492.
(15) Che, G.; Li, Z.; Zhang, H.; Cabrera, C. R. *J. Electroanal. Chem.* **1998**, *453*, 9−17.

10.1021/la702811t CCC: $40.75
Published on Web 02/01/2008

amplifying their effects (chemical amplification[16] and polymer decoration[17]) or by directly measuring them with a high-resolution microscopy technique (e.g., scanning tunneling microscopy (STM)[18] and shear force-SECM).[19] These studies have allowed one to observe different types of defects on derivatized Au(111) electrodes, including pinholes (2−3 nm diameter), and even with methods known to decrease defect density, it appears to be impossible to produce a defect-free SAM. For example, a study of SAMs on evaporated Au electrodes found a minimum pinhole density of 500 pinholes/cm^2 despite the rigorous conditions of their experiments.[16] A study of the effect of annealing SAMs with physisorbed methylene blue (MB) concluded that the ET for MB reduction was predominantly through pinholes.[20,21]

An alternative approach is to use electroactive SAMs, which feature a redox moiety (e.g., ferrocene or ruthenium bipyridine) bound to the terminal end of the alkylthiol, with the other, linking, end attached to the surfaces of metal electrodes via a S atom. Studies of these molecules are usually carried out with the electroactive thiols diluted in a mixed SAM with nonelectroactive thiols.[3] In electroactive SAMs, the redox moiety is located at well-defined distances from the electrode, and the pinhole problem is largely eliminated. The electronic coupling (and consequently, the rate of ET) between an attached redox moiety and an electrode has been shown to depend strongly on the nature of chemical bonding within the bridge,[22] by measurements of ET rates with transient techniques such as chronoamperometry[4] and CV (following changes in the peak potential with scan rate).[23] After evaluation of the coverage, Γ, rate constants of electroactive SAMs provide a straightforward way to measure the rate constant of tunneling through the monolayer (k_T in s^{-1}). Since tunneling to the redox moiety is a function of the electrode potential, a standard rate constant for the tunneling can be obtained (k^o_T in s^{-1}) with a corresponding value for α.

Electrochemical experiments on SAMs are usually carried out with Au electrodes, either fabricated from end cut wires, or vapor deposited on a substrate (e.g., glass or Si), or with single-crystal electrodes. In general, the surface of the Au is not atomically smooth over areas larger than a few hundred square nanometers, and even in the case of single crystals, step edges and domain boundaries are observed. Mercury, however, is atomically smooth, and the literature of electrochemical studies with SAMs on Hg has been reviewed.[11] Recently, a direct comparison of the results for the same electroactive moiety between the rate constants for electroactive monolayers and through an inert monolayer to a solution species has been reported.[24]

In this paper, we present a SECM study of ET as a function of electrochemical potential. Blocking monolayers of alkanethiols and electroactive monolayers of linear and norbornylous (NB) bridge systems are presented. The pinhole contribution for ET to the solution species is addressed, and a model to correct the data based on the measured α is proposed. The variability in our measurements and of literature data is discussed in terms of the pinhole contribution. Scanning electron microscopy (SEM) of electrodeposited Pd nanoparticles provides independent evidence of the presence of pinholes on a SAM.

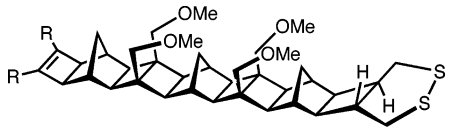

PNB: R = CONHCH$_2$Fc

Figure 1. Structure of the thiol-ferrocenyl functionalized poly-norbornylogous bridge PNBB.

Experimental Procedures

Materials. Alkanethiols ($C_9H_{10}SH$, $C_{11}H_{21}SH$, $C_{12}H_{25}SH$, and $C_{16}H_{33}SH$, Aldrich) were used as received. $Ru(NH_3)_6Cl_2$ (99.9%, Alfa Aesar) and $Ru(NH_3)_6Cl_3$ (99%, Strem Chemicals) were used as received. All other chemicals used were analytical-reagent grade. Water (18 MΩ cm) was obtained from a Milli-Q purification system (Millipore). The poly-norbornylous compounds used, shown in Figure 1, blocking PNB and ferrocene-terminated PNB, were prepared as previously reported.[25]

SECM tips were Pt in glass disk electrodes with a of 12.5 μm and RG (RG is the ratio of the insulating glass, r_g, to that of the metal electrode a, so RG = r_g/a) ∼3−5 fabricated as previously described[26] from 25 μm diameter Pt wire (Goodfellow). These tips were polished with 0.05 μm alumina before each experiment. Gold coated silicon wafers (Aldrich) with a 1000 Å thick gold layer were secured to the bottom of a Teflon cell with an O-ring that defined the electrode area as 0.272 cm^2. In experiments of SAMs on Hg, triply distilled Hg (Bethlehem Apparatus) was used to form an electrode over a 2 mm diameter Pt electrode (CH Instruments) recessed in a well of a Teflon cell (Hg area is ∼0.57 cm^2).

SAM Preparation. Gold substrates were cleaned by cycling between −0.35 and 1.4 V versus Ag/AgCl in 0.5 M H_2SO_4 at a scan rate, ν, of 0.1 V s^{-1} until reproducible scans were recorded (typically 40 cycles). To prepare SAMs of $C_9H_{10}SH$, $C_{11}H_{23}SH$, $C_{12}H_{25}SH$, and $C_{16}H_{33}SH$, the gold substrate was incubated at room temperature under a 1 mM ethanolic solution of the thiol overnight. Electroactive SAMs were prepared in two steps. In the first step, the monolayer of PNB was prepared with a solution of 1 mM PNB and 20 mM 1-undecanethiol in DMF for 30 min. The same procedure was followed for $HS(CH_2)_{14}CONHCH_2Fc$ using EtOH as the solvent and C11 as the diluent thiol. In the second step, after washing with copious amounts of the solvent and drying under a stream of argon or nitrogen, the mixed SAMS were annealed by incubation in 1 mM 1-undecanethiol in EtOH, at least overnight, and for up to 1 week. SAMs were tested by comparing the CVs of $Ru(NH_3)_6^{3+/2+}$ before and after modification of the electrodes looking for a current decrease of at least 95%.

SECM and CV Experiments. Electrochemical experiments including CV and SECM were carried out using a CHI-900A or B SECM (CH Instruments) employing a three-electrode cell with gold working electrode, platinum wire counter electrode, and Ag/AgCl (3 M KCl) as the reference electrode. All potentials are reported with respect to this reference unless otherwise stated. $Ru(NH_3)_6^{3+}$ solutions were purged with Ar before measurements and kept under an Ar blanket. For $Ru(NH_3)_6^{2+}$ experiments, a home-built SECM was used with the stage and the cell inside an Ar filled glove box to prevent air oxidation.[27]

Kinetic measurements were performed as previously reported[14] with the tip held at a potential for a diffusion-limited current at the

(16) Zhao, X. M.; Wilbur, J. L.; Whitesides, G. M. *Langmuir* **1996**, *12*, 3257−3264.
(17) Losic, D.; Shapter, J. G.; Gooding, J. J. *J. Solid State Electrochem.* **2005**, *8*, 512−519.
(18) Vericat, C.; Vela, M. E.; Salvarezza, R. C. *Phys. Chem. Chem. Phys.* **2005**, *7*, 3258−3268.
(19) Yamada, H.; Ogata, M.; Koike, T. *Langmuir* **2006**, *22*, 7923−7927.
(20) Vericat, C.; Remes Lenicov, F.; Tanco, S.; Anreasen, G.; Vela, M. E.; Salvarezza, R. C. *J. Phys. Chem. B* **2002**, *106*, 9114−9121.
(21) Benítez, G.; Vericat, C.; Tanco, S.; Remes Lenicov, F.; Castez, M. F.; Vela, M. E.; Salvarezza, R. C. *Langmuir* **2004**, *20*, 5030−5037.
(22) Sachs, S. B.; Dudek, S. P.; Hsung, R. P.; Sita, L. R.; Smalley, J. F.; Newton, M. D.; Feldberg, S. W.; Chidsey, C. E. D. *J. Am. Chem. Soc.* **1997**, *119*, 10563−10564.
(23) Laviron, E. J. *J. Electroanal. Chem.* **1979**, *101*, 19−28.
(24) Smalley, J. F.; Newton, M. D.; Feldberg, S. W. *J. Electroanal. Chem.* **2006**, *589*, 1−6.
(25) Liu, J.; Gooding, J. J.; Paddon-Row, P. N. *Chem. Commun*. **2005**, 631−633.
(26) Fan, F.-R. F.; Demaille, C. The preparation of tips for scanning electrochemical microscopy. In *Scanning Electrochemical Microscopy*; Bard, A. J.; Mirkin, M. V., Eds.; Marcel Dekker: New York, 2001; pp 75−110.
(27) Wipf, D. O.; Bard, A. J. *Anal. Chem*. **1992**, *64*, 1362−1367.

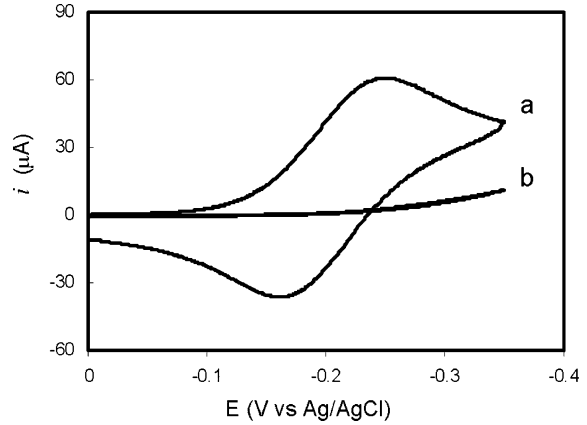

Figure 2. Cyclic voltammograms of 1 mM $Ru(NH_3)_6^{3+}$, 0.1 M NaH_2PO_4 buffer, pH 7.0 (N_2 saturated) at (a) bare gold electrode and (b) C16/Au. $\nu = 0.05$ V s^{-1} and $A = 0.283$ cm^2.

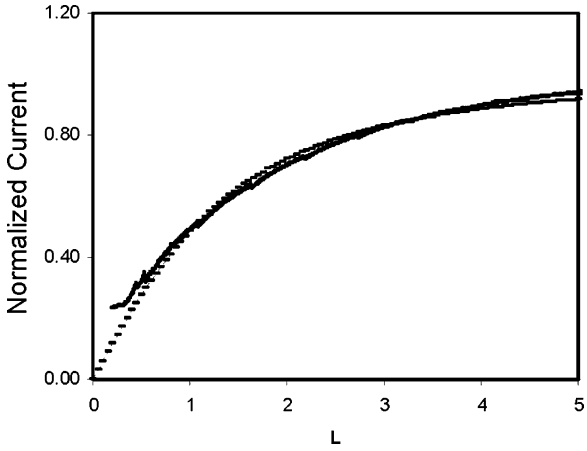

Figure 3. Approach curve in 1 mM $Ru(NH_3)_6^{3+}$ at the surface of C16/Au with $E_{subs} = 0$ V vs Ag/AgCl showing the best fit of the experimental data to the theoretical curve of negative feedback ($E_{tip} = -0.35$ V). Tip of 25 μm diameter Pt disk, supporting electrolyte 0.1 M Na_2HPO4 adjusted to pH 7.0.

tip. The tip was located above the center of the substrate and then was moved toward the surface to monitor the current as a function of position (an approach curve). Approach curves with the substrate at an open circuit generally fit the theory for pure negative feedback, which corresponds to an insulating surface blocking diffusion of the redox mediator generated at the tip. This allowed determination of the substrate position relative to the tip coordinates ($z = 0$). When a sufficient overpotential was applied to the substrate, the approach curves deviated from the negative feedback equation as the substrate and tip current became dominated by the kinetics of ET at the substrate. Approach curves were collected as a function of potential until the curves were indistinguishable from those for the pure positive feedback equation (conductive substrate), which indicates that the tip and substrate current were limited by diffusion of the redox couple in the tip−substrate gap. This procedure was carried out at the same region on the substrate to obtain one family of k_f values as a function of E, as described next. The z equals 0 position was kept approximately constant through the fitting of kinetically controlled curves and was used to compensate for any drift. The data were fit to the kinetic theory to obtain the ET rate constant at each potential. For blocking monolayers, the rate constants (k_f equals k_{ML}) obtained at one region of the substrate were fit to the Butler−Volmer equation to obtain both k^o_{ML} and α

$$k_{ML} = k^o_{ML} \exp[-\alpha f(E - E^o)] \quad (1)$$

This procedure was repeated for the blocking monolayer experiments with a $Ru(NH_3)_6^{3+}$ solution on three different regions of the substrate,

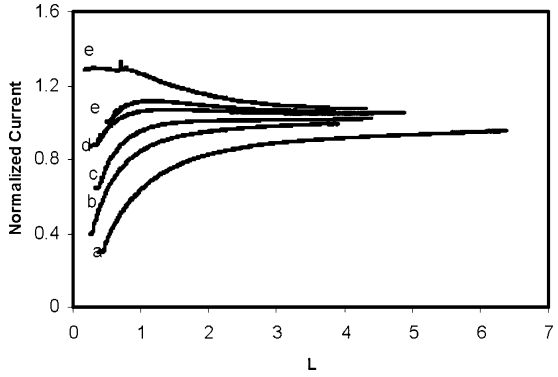

Figure 4. Approach curve in 1 mM $Ru(NH_3)_6^{3+}$ toward a C12-modified Au electrode at substrate potentials of (a) 0.0 V, (b) 0.1 V, (c) 0.3 V, (d) 0.4 V, (e) 0.5 V, and (f) 0.6 V vs Ag/AgCl. All other conditions as in Figure 3.

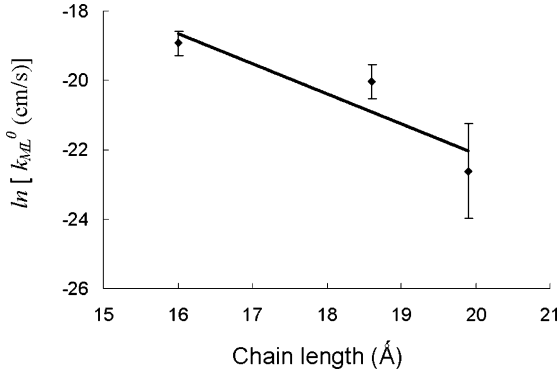

Figure 5. Standard rate constants, k^o_{ML}, corrected for pinhole contribution as a function of SAM thickness. Bars represent intervals for 95% confidence. Fitting parameters: $\ln k^o_{ML} = -0.87d - 4.73$; $R^2 = 0.83$. Experimental conditions as in Figure 3.

and the confidence intervals were calculated. Note that with the $Ru(NH_3)_6^{3+}$ solution, the tip reduces the species to $Ru(NH_3)_6^{2+}$, while the substrate oxidizes $Ru(NH_3)_6^{2+}$ back to the 3+ state. Thus, the overpotential increases in the positive potential direction. On the other hand, in the experiments with $Ru(NH_3)_6^{2+}$ solutions, the tip oxidizes the mediator to $Ru(NH_3)_6^{3+}$, while the substrate reduces it back to the $Ru(NH_3)_6^{2+}$ state. In the latter case, the overpotential increases in the negative potential direction.

Kinetic rate constants for electroactive monolayers were obtained with three different concentrations of $Ru(NH_3)_6^{3+}$ (c^o) to extract the rate constant. The measured rate constant, k_{subs} equals k_{eff}, at a given potential is

$$k_{eff} = k_T \Gamma^*/c^o \quad (2)$$

where k_T is the tunneling rate constant, Γ^* is the surface coverage of the electroactive SAM, and c^o is the concentration of the redox mediator. k_T versus the overpotential was fit to the Butler−Volmer equation to obtain k^o_T and α.

Results and Discussion

SAMs of Alkanethiols. As shown earlier,[14] SECM has several advantages in the measurement of redox kinetics through SAMs. It is a steady-state technique, so contributions from double layer capacitive charging are eliminated. Furthermore, SECM measures the redox mediator in a feedback loop; thus, any background processes that could occur on the surface (e.g., substrate oxidation or H^+ reduction) will not contribute to the faradaic current measured by the tip that is used for the measurements. These two features are key, as will be discussed later, because ET processes at pinholes can contribute to the kinetic measurements. In addition,

Table 1. Rate Constants for $Ru(NH_3)_6^{2+/3+}$ Couple via Oxidation of the 2+ Form at the *n*-Alkanethiol SAM-Covered Au Surface[a]

SAM	uncorrected k^o_{ML} (cm/s)	uncorrected α	corrected k^o_{ML} (cm/s)[b]	$\Theta_{pin}k_{pin}$
C9	$(2 \pm 1) \times 10^{-4}$	0.15 ± 0.02	$(6 \pm 2) \times 10^{-9}$	$(8 \pm 1) \times 10^{-3}$
C11	$(3.8 \pm 0.7) \times 10^{-5}$	0.17 ± 0.02	$(1.5 \pm 1) \times 10^{-9}$	$(2 \pm 1) \times 10^{-3}$
C12	$(1.2 \pm 0.2) \times 10^{-4}$	0.09 ± 0.02	$(1.5 \pm 3) \times 10^{-10}$	$(9 \pm 4) \times 10^{-4}$

[a] Averages of three measurements and a confidence level of 95%. [b] Corrected by assuming a constant pinhole current, see text.

Table 2. Summary of Kinetic Data for Solution-Phase $Ru(NH_3)_6^{2+/3+}$ on Alkanethiol-Modified Electrodes

SAM	*d* (Å)[a]	technique	k^o_{ML} (cm/s) Au	Hg	α	Au(*hlk*)	ref[f]
C9	16	IS	9.21×10^{-5}		0.48	(111)	10
		IS	9.35×10^{-5}		0.49	(210)	10
HO-C11		*b*	1.4×10^{-5}				*b*
C12	19.9	potentiometry		2.16×10^{-7}	*c*		12
		IS	1.08×10^{-6}		0.57	(111)	10
		IS	2.13×10^{-6}		0.55	(210)	10
		SECM	1.0×10^{-8}	2.4×10^{-10}	0.6	this work	
C16	25.1	potentiometry		1.42×10^{-9}			12
		CV		3.00×10^{-13}	*c*		8
		IS	1.44×10^{-7}		0.51	(111)	10
		IS	2.75×10^{-7}		0.55	(210)	10
HO-C16		CV[d]	6.38×10^{-9}		0.26	evaporated	7
C18	27.7	IS[e]		4.98×10^{-7}	*c*		11
		potentiometry		2.14×10^{-10}			12
		IS	3.28×10^{-8}		0.49	(111)	10
		IS	3.58×10^{-8}		0.52	(210)	10

[a] Calculated according to eq 4 as suggested in ref 3. [b] C. J. Miller and J. I. Blankman, unpublished results reported in ref 24 for $HO(CH_2)_{11}SH$. [c] α is assumed to be 0.5 for k^o calculations in these reports. [d] Calculated from the data for $HO(CH_2)_{16}SH$ in Figure 3, ref 7. [e] Calculated from $k_{CT} = 1.08 \times 10^{-8}$ Ω. [f] Ref 7: thermally evaporated Au on Cr/Si, incubated in saturated aqueous $HO(CH_2)_{16}SH$ + 50 mM decyltrimethylammonium bromide at its reflux point. Ref 8: SMDE incubated in 20% (v/v) thiol in *n*-hexadecane, 2 s to 30 min at OCP. k^o_{ML} measured in 5 mM $Ru(NH_3)_6Cl_3$ and 0.1 M NaF. Ref 10: electrode incubated in 30 mM thiol in EtOH for 16 h at OCP; k^o_{ML} measured at 25 ± 1 °C, 1 mM $Ru(NH_3)_6[ClO_4]_3$/0.1 M $NaClO_4$. Ref 11: HMDE in 5 mM thiol in EtOH for 30 min at OCP; k^o_{ML} measured in 1 mM $Ru(NH_3)_6Cl_3$/0.1 M KNO_3 $E_{app} = E^{o\prime}$. Ref 12: HMDE incubated in 5 mM thiol in EtOH for 30 min at OCP; k^o_{ML} measured $E(t)$ in $Ru(NH_3)_6Cl_3/Ru(NH_3)_6Cl_2$/0.1 M KNO_3.

the use of an UME as a tip makes the *iR* drop negligible (i_{tip} is ~1−10 nA), and a wider range of substrate potentials (i.e., overpotentials) is available in SECM as compared to CV.

CV can be used to judge the bulk electrochemical behavior of a SAM-modified substrate. Figure 2 shows typical CV images of 1 mM $Ru(NH_3)_6^{3+}$ at the surface of a gold substrate before and after modification with 1-hexadecanethiol (C16). $Ru(NH_3)_6^{3+}$ shows quasi-reversible electrochemical behavior at the bare gold electrode. The CV image of $Ru(NH_3)_6^{3+}$ at the surface of the monolayer (Figure 2b) shows, from the decrease in redox current, that the ET between electrode surface and tip-generated $Ru(NH_3)_6^{2+}$ was effectively hindered by the C16 SAM. If the $Ru(NH_3)_6^{2+}$ probe molecules cannot penetrate the monolayer framework, they can only be oxidized by tunneling through the C16 layer. Figure 3 shows a SECM approach curve (E_T is −0.35 V vs Ag/AgCl) to a C16/Au sample at a substrate potential, E_S, of 0 V vs Ag/AgCl. The feedback from the substrate due to ET through the SAM was negligible because the experimental curve matches the negative feedback theory. This is consistent with the CV experiments (Figure 2b) with the C16-derivitized electrode: an effectively blocking SAM will hinder redox reactions at potentials where tunneling through the SAM is slow. These sluggish redox kinetics translate to currents near the baseline in the CV image (Figure 2b) and to SECM approach curves that are close to negative feedback theory (Figure 3) (i.e., the case of a purely insulating or blocking surface). For C16, it was not possible to perform kinetic measurements since the negative feedback response did not change for E_S values up to 1.3 V vs Ag/AgCl. Increasing E_S to more positive values resulted in the removal of the SAM, resulting in positive feedback from the substrate. Dodecanethiol (C12) studies with $Ru(NH_3)_6^{3+}$ in solution are shown in Figure 4. As E_S was varied from 0 to 0.6 V versus Ag/AgCl, the rate of $Ru(NH_3)_6^{2+}$ oxidation through the SAM increased, and the approach curves changed from negative feedback to positive feedback. The rate constants obtained were fit to eq 1 and a k^o_{ML} value of $(1.2 \pm 0.2) \times 10^{-4}$ cm/s and an α value of 0.09 ± 0.02 were obtained. When the incubation time for forming the SAM was increased to 2 weeks, k^o_{ML} decreased to 3×10^{-5} cm/s, and α increased to 0.11. Similar measurements were performed for 1-undecanethiol (C11), and 1-nonanethiol (C9), and the results are presented in Table 1. Note that the α values are small as compared to 0.5 and that the k^o_{ML} values do not correlate with the number of carbons in the chain (tunneling distance). Similar findings have been reported in earlier studies.[6] We propose that some contribution of species that reacts at pinholes in the film affects these results and causes an anomalously small value of α and is consistent with the finding that increasing the incubation time increases the value of α. The contribution from pinholes in SAMs prepared with the same procedure varied from sample to sample because the size and number of defects depend on factors such as the substrate structure and cleanliness, temperature, thiol concentration, and incubation time. Samples imaged by high-resolution scanning probe techniques show differences between samples and even within the same sample,[20,21] so it is difficult to correct kinetic data for pinhole effects.

In the SECM and CV experiments, the pinhole contribution led to an overestimation in the rate of ET of blocking monolayers. To correct for these effects, it is necessary to use a method that accounts for the wide variability of pinhole sizes and their distribution. An alternative to this problem is the use of a redox-terminated SAM, usually diluted with nonelectroactive molecules, which are less sensitive to defects and pinholes in the monolayer.

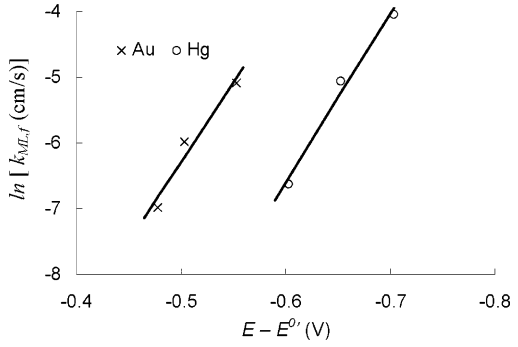

Figure 6. Rate constants for $Ru(NH_3)_6^{3+/2+}$ measured on C12 on Hg and Au. Fitting to the Butler−Volmer equation for Au: $k^o_{ML} = 1.01 \times 10^{-8}$, $\alpha = 0.62$, $R^2 = 0.95$ and for Hg: $k^o_{ML} = 2.38 \times 10^{-10}$, $\alpha = 0.67$, $R^2 = 0.95$. 2.5 mM $Ru(NH_3)_6Cl_2$ in 0.1 M Na_2HPO_4 at pH 7.0 in Ar atmosphere, 25 μm diameter Pt tip. See Supporting Information for more details.

However, it is also of interest to compare the values of the ET and direct tunneling rate constants for the same chain structure and length from blocking and electroactive SAMs.[24] To compare rate constants between them or with theoretical models requires accurate knowledge of the rate constants and thus correction for pinhole effects.

Pinholes provide a parallel path to the current through the monolayer following the equation for the total current across a monolayer, eq 3[14]

$$i = \theta nFAk^o_{ML}C_o(0,t)\exp(-\alpha_{ML}\eta f) + (1-\theta)nFAk^o_{pin}C_o(0,t)\exp(-\alpha_{pin}\eta f) \quad (3)$$

where θ is the monolayer coverage. Assuming that $\alpha_{ML} = \alpha_{pin} = 0.5$, the relative ratio of the contribution i_{pin}/i_{ML} is $(1-\theta)$-$k^o_{pin}/\theta k^o_{ML}$. Assuming that k^o_{ML} is $\sim 10^{-3}$ cm/s and that k^o_{pin} is $\sim$1 cm/s, from the previous equation, one can see that to make i_{ML} equal to $\sim 10 i_{pin}$, then $(1-\theta)/\theta$ must be on the order of 10^{-4}, which corresponds to a very high monolayer coverage. The actual values of k^o_{pin} for the pinhole and k^o_{ML} monolayer are the subject of current investigation, but for the SAMs in this work, literature values for k^o_{ML} are on the order of 10^{-5} cm/s or lower (Table 2).

According to eq 3, pinholes will have the effect of significantly increasing the measured apparent constant at any given potential. The pinhole current increases exponentially until it becomes limited by mass transport. At large overpotentials, pinholes operate as an array of UMEs at their diffusion-limited current.[3,15] This will contribute a significant offset current that is constant with overpotential, so that the apparent value of α for the SAM will appear smaller. A similar model was proposed by Finklea et al.[28] for "collapsed sites in the monolayer", which suggested that the rate constant varied greatly across the surface. A simulation of this model was used to show that a smaller value of α could be due to the distribution of rate constants across the sample, although, to the best of our knowledge, no attempt has been made to extract rate constants using this model. Protsailo et al.[10] have accounted for the defect contribution by adding two parallel paths: a resistor, R_{SAM}, attributed to pinholes and defects, and a constant phase element (CPE, to simulate double layer effects), both in parallel to the faradaic impedances of charge transfer (R_{ct}) and diffusion (Warburg). Addition of parallel paths for the current results in a correction for R_{ct} and of k_{ML}. The dependence of k_{ML} with potential fit the Butler−Volmer equation with α equals 0.5.

(28) Finklea, H. O.; Avery, S.; Lynch, M. *Langmuir* **1987**, *3*, 409−413.

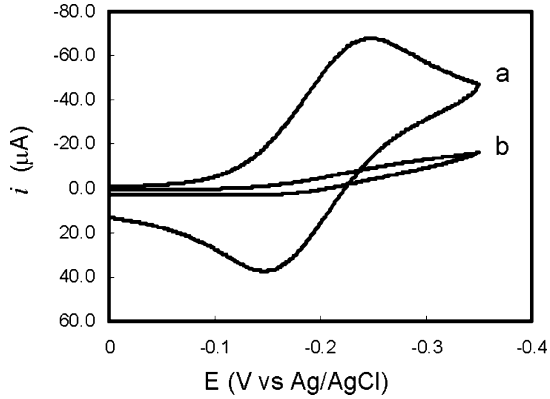

Figure 7. Cyclic voltammograms in 1 mM $Ru(NH_3)_6^{3+}$ to the surface of (a) bare gold electrode and (b) SAMs on PNB. Same conditions as in Figure 2, $\nu = 0.05$ V s^{-1} and $A = 0.2826$ cm^2.

To compensate for pinhole contributions in the SECM measurements, we assume that this contribution essentially reaches a limiting value at the potentials where the kinetics of monolayer transfer is measured. Thus, a constant value for this contribution of pinhole current was subtracted from the measured rate constants at all potentials to yield an α value of 0.5. The result of this correction is shown in Table 1.

A logarithmic plot of the corrected k^o_{ML} values versus alkanethiol length is shown in Figure 5. The length was calculated from the number of methylene groups, n_{CH_2} according to[3]

$$d\ (\text{Å}) = 5.6 + 1.3n_{CH_2} \quad (4)$$

The rate constants follow the expected trend: a decrease exponentially as the distance increases. Fitting the data to an equation in the form of eq 5 yields β equals 0.87 $Å^{-1}$, which is in reasonable agreement with the reported β value of $\sim$1 for saturated chains

$$k^o_{ML} = k_B(0)\exp[-\beta d] \quad (5)$$

It should be noted that distances from eq 4 neglect the effect of the tilt angle on the SAMs and that correlating the rate constant to this distance is equivalent to assuming that tunneling occurs through the fully extended molecule. Because of the scatter of the experimental results and the small number of points, it is not possible to assess the contribution of through-space tunneling due to the known tilt of the SAMs (ca. 30° with respect to the Au substrate plane).[2,3] Note that the dispersion in our data is due to the variability of the rate constant across individual samples and that this surface distribution data are available from using SECM. Also, statistical evaluation of confidence levels using a Student's t test is usually not reported in the literature, and treatments of the tilt angle effect on ET assume a perfect monolayer. In summary, our approach corrects for pinhole contribution and yields standard rate constants that are 3−4 orders of magnitude smaller than those obtained assuming perfect SAMs. These corrected rate constants follow the expected distance dependence of tunneling through a blocking medium. To the best of our knowledge, there are only a few reports on the standard rate constant dependence on alkanethiol length, although rate constants at high overpotentials follow this relationship. Protsailo et al.[10] reported different values of k^o_{ML} (calculated for a model including defects) for SAMs (C9, C12, C16, and C18) on different crystalline planes, but they observed similar decay constants for Au(111) (β is 0.83 $Å^{-1}$) and for Au(210) (β is 0.87 $Å^{-1}$). On Hg, with no pinhole contribution, Cohen-Atiya et al.[11] reported

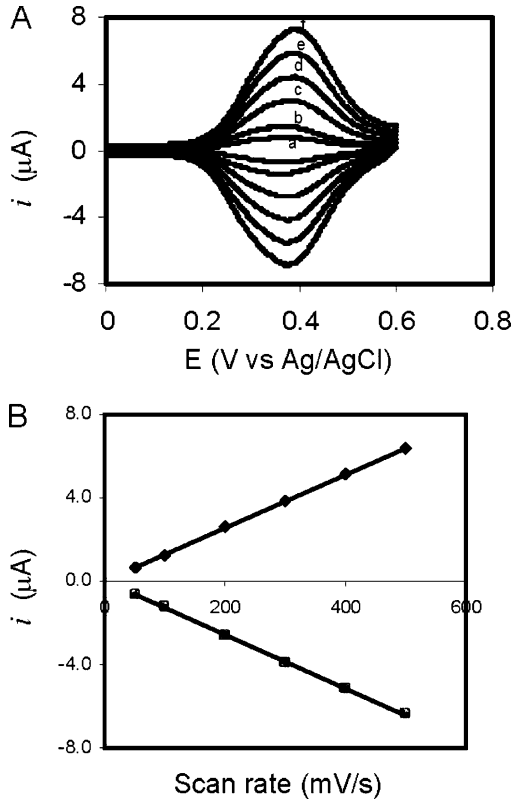

Figure 8. (a) Cyclic voltammograms of SAMs of PNB and C11 (diluent)/Au in 0.1 M phosphate buffer (pH 7.0) at scan rates (a−f) $\nu = 0.05$, 0.1, 0.2, 0.3, 0.4, and 0.5 V s^{-1} and (b) plot of anodic and cathodic peak current vs scan rate.

standard rate constants for alkanethiols following this exponential decay with β of 0.9 $Å^{-1}$, and Calvante et al.[29] reported β of 0.9 $Å^{-1}$ for ω-hydroxylalkanethiols.

Table 2 shows a compilation of data taken from the literature for the kinetics of the $Ru(NH_3)_6^{3+/2+}$ couple at alkanethiols covering single-crystal Au and Hg surfaces. For Au electrodes, our corrected values for k^o_{ML} are 3−4 orders of magnitude smaller than those reported for Au single crystals. Table 2 also includes k^o_{ML} data reported on Hg. Despite the dispersion of the k^o_{ML} values for alkanethiols, k^o_{ML} values measured on Hg electrodes are in general 1−2 orders of magnitude smaller than those of Au. This difference has been attributed to a much smaller defect density of alkanethiol SAMs formed on Hg than on Au.[8−12] As originally proposed by Demoz and Harrison,[8] alkanethiol molecular interactions favor the formation of a densely packed SAM on the atomically smooth Hg surface. We attempted to measure the kinetics of $Ru(NH_3)_6^{2+/3+}$ oxidation on C12/Hg with SECM (with the tip generating the 2+ species from the 3+ in bulk solution), but applying a substrate potential of +0.5 V versus Ag/AgCl, the onset of Hg oxidation in Cl^- and PO_4^{3-}, producing an insulating film, yielded approach curves showing negative feedback. If the system is changed to one where the reduced species $Ru(NH_3)_6^{2+}$ is used in a solution kept free from oxygen, $Ru(NH_3)_6^{2+}$ is oxidized at the tip to the 3+ state, and the rate of the reduction to the 2+ species at the substrate is measured. With this setup, large negative overpotentials could be used at the substrate (an important advantage of SECM over CV measurements); results are shown in Figure 6 for Hg and Au substrates. Note that in determining the rate constant from SECM approach curves, those curves that are near to those of an insulating

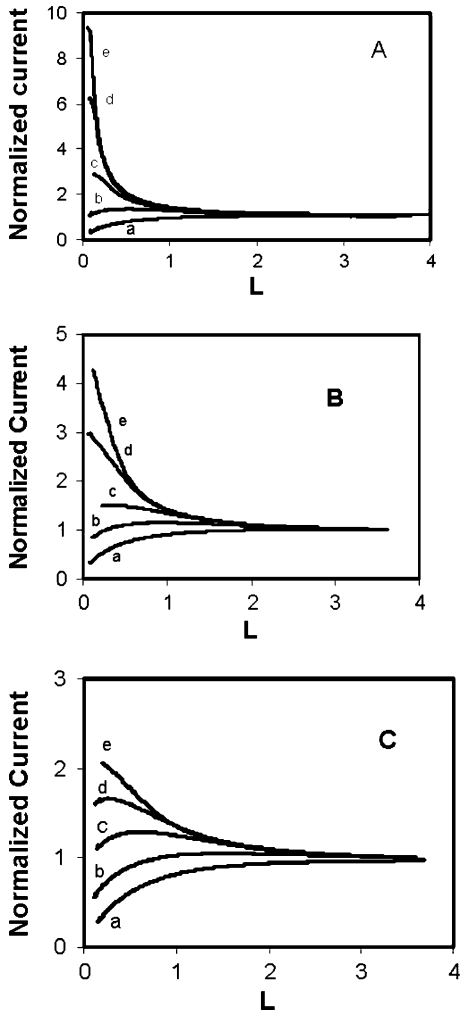

Figure 9. Typical approach curves for different concentrations of $Ru(NH_3)_6^{3+}$ [(A) 1.3 mM, (B) 2.3 mM, and (C) 5.6 mM] to the surface of SAMs at different substrate potentials: (a) 0.10 V, (b) 0.30 V, (c) 0.40 V, (d) 0.45 V, and (e) 0.48 V. $E_{tip} = -0.35$ V vs Ag/AgCl, tip of 25 μm diameter Pt disk, supporting electrolyte 0.1 M Na_2HPO_4 at pH 7.0.

substrate for very small rate constants (total negative feedback) or for diffusion controlled positive feedback for very high rate constants cannot be measured with good precision because of the inevitable uncertainty in the $d = 0$ position. In Figure 6, we only show the data with the most reliable kinetic information (i.e., rate constants obtained from approach curves intermediate between positive and negative feedback and curves that show a maximum). The complete data set is shown in the Supporting Information. Supporting Information Figure S1 shows the same trend for Hg and Au; an initial limiting value for k_{subs}, largely attributed to pinholes, is attained at low overpotentials, and at larger overpotentials, the rate begins to increase exponentially due to the k_{ML} contribution. The pinhole contribution in these cases appears to be much smaller. On Hg, this is expected from a better SAM packing on the atomically smooth surface. We are unsure of the reason for this on Au, but apparently we obtained a SAM with an unusually high coverage from a long incubation (2 weeks) in the thiol solution. k^o_{ML} was calculated taking the three most negative overpotentials (Figure 6) and fitting them to the Butler−Volmer eq 1. For Au, k^o_{ML} was 1×10^{-8} (σ equals $\pm 3 \times 10^{-8}$) and α was 0.62. For Hg, k^o_{ML} was 2×10^{-10} (σ equals $\pm 5 \times 10^{-10}$) and α was 0.67. There is considerable uncertainty in these results because of the long extrapolation to obtain k^o_{ML}. The standard rate constant on Au is larger than that

(29) Calvante, J. J.; López-Pérez, G.; Ramírez, P.; Fernández, H.; Zón, M. A.; Mulder, W. H.; Andreu, R. *J. Am. Chem. Soc.* **2005**, *127*, 6476−6486.

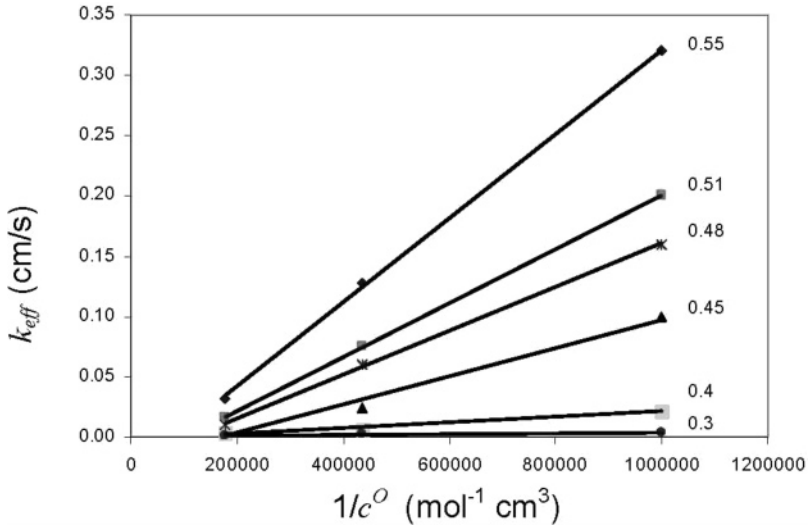

Figure 10. Dependence of k_{eff} (cm/s) on the concentration of $Ru(NH_3)_6^{3+}$ for a monolayer of PNB and C11/Au. The numbers on the plot indicate E_{subs} and $E_{tip} = -0.35$ V vs Ag/AgCl. $\Gamma = 7.58 \times 10^{-11}$ mol cm^{-2}. Same solution conditions as in Figure 9. k_{eff} values were extracted from fitting approach curves in Figure 9 to theory.

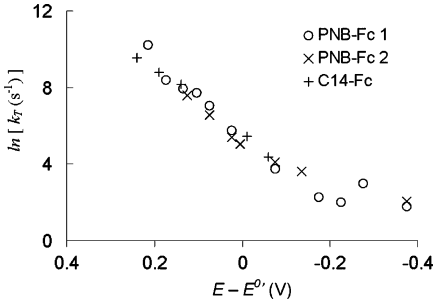

Figure 11. Dependence of k_T on overpotential for ferrocene monolayers for PNB and $FcCONHC(CH_2)_{12}SH$ sample 2 (C14-Fc). Experimental conditions as in Figures 9− and 10.

on Hg by 2 orders of magnitude. Our extrapolated result using the model for pinhole correction is 1.5×10^{-10} (σ equals $\pm 0.73 \times 10^{-10}$) for the oxidation of the mediator on C12/Au (Table 1). At larger numerical values of overpotential ($E^{0\prime}$ equals −0.2 V vs Ag/AgCl), one exceeds the potential limits for SAM stability, especially on Au, which would lead to a potential dependent increase in leakage at very negative potentials and could explain the value of α being slightly above 0.5. However, even with these problems, the apparent rate constants we find are as much as 4 orders of magnitude smaller than those reported in the literature (Table 2). Another issue is that the rate constants are expected to deviate from the exponential increase predicted by the Butler−Volmer eq 1 and to curve downward at large overpotentials with the α value decreasing from 0.5, as proposed by Chidsey in his formulation of the Marcus theory for redox SAMs.[4] This curvature is expected to decrease the rate constant by more than 20% from the Butler−Volmer equation for $\eta >$ 0.15 V, assuming for $Ru(NH_3)_6^{3+/2+}$ a reorganization energy of ∼1 V.[30] However, our most reliable kinetic data show an exponential increase for η of −0.5 to −0.7 V. Also, a value of $\alpha \leq 0.4$ is expected for $\eta \geq 0.5$ V, while it is common to observe $\alpha < 0.2$ at $|\eta| < 0.5$ V, where the Butler−Volmer equation is expected to hold with α equals 0.5. Note that our results show $k^o_{ML}(Au) \gg k^o_{ML}(Hg)$, opposite to the expected trend from the ratio of densities of states from the free-electron theory [$\rho_m(Au)/\rho_m(Hg)$ is ∼0.6];[24,30] and this trend has been reported by others (see Table 2). The general conclusion is that measurements of this type at high overpotentials are difficult and that the trend of a larger rate constant on Au as compared to Hg is probably primarily a reflection of the better quality of the SAM on Hg, as previously found.[11,12] More reliable data are needed to analyze rate constants more closely in terms of Marcus theory and the metal density of states. The measurements of C12 are about at the lower limit for the measurement of rate constant, and electrons will not tunnel through longer chains at these overpotentials (0.7 V) (see Table 2). The C16 thiol always behaved as an insulator when studied with SECM. In summary, the Butler−Volmer equation for rate constants can be used to explain the potential dependence of redox kinetics on SAMs, once the measurements are corrected for a pinhole contribution.

Electroactive SAMs. Measurements on electroactive SAMs are much less susceptible to pinholes and defects.[1,4] The drawback of CA and CV in these measurements is that the *iR* drop and charging currents can affect the results. SECM, a steady-state technique, eliminates the problems of transient backgrounds and was used to study the potential dependence of ET in ferrocene-terminated monolayers. SECM also gives the rate of reaction of the electroactive group and mediator and the extent of leakage of the mediator through the film.

Figure 7 shows CV images of $Ru(NH_3)_6^{3+}$ at the ferrocene-terminated PNBs on a Au electrode before (Figure 7a) and after incubation in PNB solution (Figure 7b). Reduction of $Ru(NH_3)_6^{3+}$ was significantly hindered by the PNB SAM but was not blocked as effectively as with C16 (compare Figures 7b and 2b). CV images from various scan rates for PNB/Au are shown in Figure 8. The redox centers at about 20 Å from the electrode surface show a redox peak with the full-width at half-maximum (ΔE_{fwhm}) of the CV image of about 190 mV. This ΔE_{fwhm} value is larger than the theoretically expected value of 91 mV at 25 °C, which may be caused by the existence of redox centers in different environments. A plot of anodic and peak current against the scan rate (Figure 8b) was linear with R^2 values of 0.9995 and 0.9996 for the anodic and cathodic peak currents, respectively, as expected for a surface confined electroactive center. The coverage of electroactive species, Γ, calculated by integration of the peak current (Figure 8a) was 7.58×10^{-11} mol (of Fc) cm^{-2}.

Figure 9 shows approach curves obtained for PNB/Au at different substrate potentials and different concentrations of $Ru(NH_3)_6^{3+}$. Increasing the substrate overpotential led to a change

(30) Feldberg, S. W.; Newton, M. D.; Smalley, J. F. *Electroanal. Chem.* **2004**, *22,* 101−180.

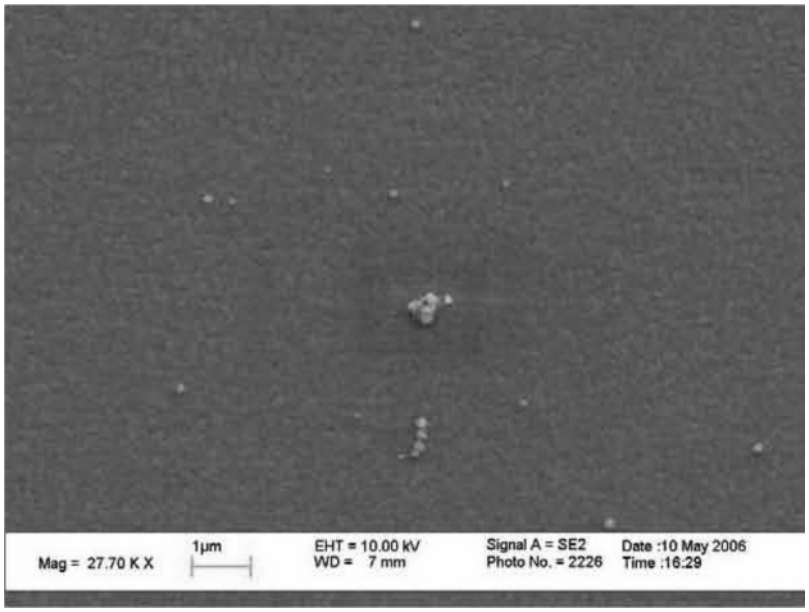

Figure 12. SEM image of C12/Au SAM after deposition of Pd particles (bright spots) at a potential of 0.34 V vs Ag/AgCl in 1 mM $PdCl_2$/0.1 M H_2SO_4 for 20 s ($A = 0.126$ cm^2).

Table 3. Standard ET Rate Constants for Ferrocene-SAMs[a]

		std rate constant (s^{-1})		transfer coefficient		
SAM	$10^{12} \times \Gamma$ (mol/cm^2)	k^o_T	σ	α	σ	R^2
		PNB				
sample 1, $N = 7$	0.8	200	38	0.54	0.04	0.987
sample 2, $N = 5$	0.7	178	22	0.46	0.04	0.986
Av		189	31	0.50	0.04	
		$HS(CH_2)_{14}CONHCH_2Fc$				
sample 1, $N = 4$,	3.7	182	19	0.25	0.02	0.996
sample 2, $N = 5$	6.4−2.5	253	27	0.44	0.02	0.998

[a] Γ is the coverage of Fc. N is the number of $k_T(E)$ measurements on the SAM.

from negative to positive feedback. When the substrate potential is above 0.3 V, the Fc moiety is oxidized to ferrocenium at a rate limited by the ET through PNB. The tip potential was set to reduce $Ru(NH_3)_6^{3+}$ at the diffusion-limited rate (E_{tip} equals −0.35 V versus Ag/AgCl). Then, $Ru(NH_3)_6^{2+}$ diffuses from the tip to the ferrocene attached to the monolayer, and $Ru(NH_3)_6^{2+}$ is oxidized by the ferrocenium, increasing the feedback current at the tip. The potential dependence of ET is evident from the change in the substrate rate constant, k_{eff}.[14] Figure 10 shows a series of plots of k_{eff} versus the reciprocal of the $Ru(NH_3)_6^{3+}$ concentration for the substrate held at different potentials. The slopes of the lines in Figure 10 are the tunneling rate constant, k_T.[14] The potential dependence of k_T follows Butler−Volmer behavior (Figure 11). This procedure was repeated (using a different sample), and fitting parameters to eq 1 are shown in Table 3. Results for $FcCH_2NHCOC_{14}SH$ (C14Fc), of the same length of PNB, are also shown, and they follow the same trend as the results for PNB. Table 3 demonstrates that the k^o_T value for the two molecules (d is ∼20 Å) are equivalent within experimental error, and on the order of k^o_T equals 189 s^{-1} with α of 0.5, as calculated for PNB. Note that sample 1 gave an anomalously small α value, we think from a pinhole contribution for this sample since substrate two, with a good blocking SAM, gave α of ∼0.5. In summary, we found that ferrocene-terminated SAMs follow the simple Butler−Volmer kinetics with α equals 0.5 and that the PNB system has the same ET rate as an alkane chain of the same length. Intriguingly, this observation is contrary to our previous ET rate measurements on PNB SAMs, using CV and alternating current voltammetry, which revealed a rate enhancement factor of at least 2 orders of magnitude greater than that through a single-chain analogue of comparable length. The reason for this discrepancy is the subject of active investigation. These measurements are within 1 order of magnitude of those of Smalley et al.[5] for $HS(CH_2)_{16}Fc^{+/o}$ (k^o_T is 28 ± 3 s^{-1}) and are consistent with those measured with SECM for shorter chains (assuming α equals 0.5).[14]

Comparing the Standard Rate Constants for Blocking and Redox SAMs. Smalley et al. proposed the use of a comparison factor, P_c, that normalizes the rates of ET through redox SAMs (k^o_T, in s^{-1}) to that of the rated constant of a blocking SAM to the same redox couple in solution (k^o_{ML} in cm/s)[24]

$$P_c = \frac{k^o_T \exp[\beta(d_A - d_S)]}{\beta_S k^o_{ML}} \quad (6)$$

where β_S is the exponential decay coefficient for aqueous solution (β_S equals 1.68 ± 0.07 Å^{-1}),[31] and d_A and d_S are the characteristic distances for ET on electroactive and blocking SAMs, respectively. From data in the literature, P_c was found to be within an order of magnitude of 1, which would indicate that the rates for bridge mediated ET to a covalently attached redox moiety ($Ru(NH_3)_5Py$- or Fc-) are the same as for a blocking SAM of the same length with the redox active species in solution. However, our electrochemical measurements indicate that SAMs of C12 (d_s equals ∼20 Å) show a much smaller heterogeneous rate

(31) Ponce, A.; Gray, H. B.; Winkler, J. R. *J. Am. Chem. Soc.* **2000**, *122*, 8187−8191.

constant for $Ru(NH_3)_6^{3+/2+}$ in solution as compared to the reported value for $HS(CH_2)_{14}COHCH_2PyRu(NH_3)_5$ (d_A equals ~21 Å) measured by CV.[32] Thus, the factor of P_c for monolayers using our k^o value for solution species and the literature value for an electroactive SAM gives a P_c value of $\sim 10^3$, closer to the expectation[24] that tunneling via bonded contacts is more efficient than tunneling to nonbonded contacts (e.g., as found in glasses).[33]

Pinhole detection on a SAM, or the estimation of the pinhole density, would allow for independent verification of the pinhole contribution. Electrodeposition of Pd was employed to deposit metal nanoparticles at pinholes that could then be observed by SEM. Pd particles were deposited at 0.34 V versus Ag/AgCl on a C12/Au sample. An SEM image of the monolayer after deposition of Pd at a constant potential is shown in Figure 12. The Pd particles (~100 nm) show the existence of pinholes in the monolayer that are not evenly distributed over the surface.

Conclusion

Electron transfer of blocking and electroactive monolayers was studied with SECM. The potential dependence of the electrochemical rate constants for blocking SAMs of $C_9H_{10}SH$, $C_{11}H_{21}SH$, $C_{12}H_{25}SH$, and $C_{16}H_{33}SH$ for $Ru(NH3)_6^{2+/3+}$ in solution was found to follow the Butler−Volmer equation, with a transfer coefficient, α, that was anomalously small. This deviation was explained in terms of a contribution from reaction at pinholes. A model for correction for the pinhole contribution yielded values of k^o that follow the expected exponential decay (β equals 0.9 A^{-1}) but that are several orders of magnitude smaller than those previously reported in the literature. Experiments on Hg for reduction of this mediator support this finding and yield an α value of 0.5.

$HS(CH_2)_{14}CONHCH_2Fc$ and Fc-terminated PNB were found to show essentially the same tunneling behavior. The tunneling rate constants also followed Butler−Volmer kinetics in the potential range that we measured here. Our results suggest that ET to a redox moiety attached to a SAM is more efficient that ET through a blocking monolayer to a redox species in solution. Finally, SEM imaging of SAM/Au after electrochemical deposition of Pd nanoparticles showed deposits consistent with the existence of pinholes and provided an idea as to their distribution.

Acknowledgment. We appreciate helpful discussions with Dr. Steve Feldberg. This research was supported by the National Science Foundation (CHE 0451494) and the Robert A. Welch Foundation. A.K. thanks the Iranian Ministry of Science, Research and Technology for financial support. The Australian group thanks the Australian Research Council for support.

Supporting Information Available: Complete data set of kinetic information for Figure 6. This material is available free of charge via the Internet at http://pubs.acs.org.

LA702811T

(32) Finklea, H. O.; Melissa, L. L.; Ravenscroft, S.; Puntura, S. *J. Phys. Chem.* **1996**, *100*, 18852−18858.

(33) Wenger, O. S.; Leigh, B. S.; Villahermosa, R. M.; Gray, H. B.; Winkler, J. R. *Science (Washington, DC, U.S.)* **2005**, *307*, 99.